Journal of Power Sources 187 (2009) 461–470

Contents lists available at ScienceDirect

Journal of Power Sources

journal homepage: www.elsevier.com/locate/jpowsour

Electrokinetic energy conversion efficiency analysis using nanoscale finite-length surface-charged capillaries

Reiyu Chein*, Chencheng Liao, Hongjie Chen

Department of Mechanical Engineering, National Chung Hsing University, Taichung 402, Taiwan

ARTICLE INFO

Article history:
Received 19 September 2008
Received in revised form 28 October 2008
Accepted 5 November 2008
Available online 13 November 2008

Keywords:
Electrokinetic effect
Surface charge density
Electrostatic potential gradient
Energy conversion efficiency
Dimensionless Debye length

ABSTRACT

Electrokinetic power generation efficiency using a two-dimensional axisymmetrical model is numerically investigated. A finite-length nanoscale surface-charged cylindrical capillary with reservoirs connected at the capillary ends is considered as the physical domain. The Navier–Stokes, Laplace, Poisson, and Nernst–Planck equations are solved simultaneously to obtain the fluid flow, electrical potential, ion concentration and electrical current in the flow field. The energy conversion efficiency predicted using a one-dimensional model assuming an infinitely long channel, Boltzmann ion distribution and equal ionic electrical mobility is also carried out and compared with the two-dimensional result.

The two-dimensional model results show that the electrostatic potential gradient resulting from the concentration changes at the capillary entrance and exit and fluid flow produce a conductive current that reduces the total current in the flow field. The conductive current due to the electrostatic potential gradient increases with the decrease in electrolyte bulk concentration and increase in surface charge density. This results in nonlinear variations in the electric current–voltage curve and maximum conversion efficiency as functions of the surface charge density and dimensionless Debye length when the electrolyte bulk concentration is low. Comparison of the maximum efficiencies predicted from one- and two-dimensional models indicates that the one-dimensional model is valid only when the dimensionless Debye length is large and the surface charge density is small because the electrostatic potential gradient is neglected. The two-dimensional model also predicts that optimum maximum energy conversion efficiency can be obtained when the dimensionless Debye length is equal to 2 and its magnitude increases with the increase in surface charge density.

1. Introduction

Because of the developments in recent microfabrication technology, micro or nanoscale channels have become available, playing an important role in many engineering applications. For example, fluid transport in nanoscale fluidic systems by applying an external electrical field is used for chemical and biological analyses in the lab-on-a-chip devices [1–3]. Besides chemical and biological analyses, micro and nanoscale fluidic system applications in energy conversion based on electrokinetic effects have recently gained much interest in the research society because of the demand for finding new and environmental-friendly energy resources [4,5].

The electrokinetic energy conversion principle utilizes two fundamental electrokinetic effects: the streaming potential and electroosmosis. These two phenomena rely on the existence of an electrical double layer (EDL) near a channel wall. The theories regarding the formation of EDL, electroosmosis and streaming potential are well documented in several textbooks [6–8]. This is based on the fact that most surfaces are electrically charged when they are brought into contact with a polar medium such as an aqueous electrolyte. Because of the charged surface, preferentially distributed counter-ions and co-ions are created near the surface. The ion distribution combined with random thermal motion results in EDL formation. As the fluid flow is driven by an externally applied pressure gradient, the fluid flow carries the ions to the channel downstream. The charge transport results in an electric current, known as the streaming current. The charge polarization due to accumulated ions at the channel downstream creates an electrical potential difference between the channel ends and a conductive current with a direction opposite to the flow direction. The electrical potential difference is termed the streaming potential because it is created by the fluid flow. The streaming potential theory has recently been applied to build an electric power generation unit since the maximum streaming potential can be regarded as an open circuit potential (or the electromotive force) similar to that in an electrochemical cell [9–14]. Because of this similarity, electric power generation based on the streaming potential theory may be termed the "Electrokinetic Cell" (EK cell).

* Corresponding author. Tel.: +886 4 22840433/22870195; fax: +886 4 22877170.
E-mail address: rychein@dragon.nchu.edu.tw (R. Chein).

0378-7753/$ – see front matter © 2008 Elsevier B.V. All rights reserved.
doi:10.1016/j.jpowsour.2008.11.010

Nomenclature

a	radius of cylindrical capillary (m)
A_R	radius of computational domain in reservoirs (m)
c_0	bulk electrolyte molar concentration, M (mol L^{-1})
D	molecular diffusivity ($m^2\ s^{-1}$)
F	Faraday constant (96,500 C mol^{-1})
G	hydrodynamic conductance ($m^3\ Pa^{-1}\ s^{-1}$)
L	length of cylindrical capillary (m)
L_R	length of computation domains in reservoirs (m)
m	electrical mobility (mol s kg^{-1})
M	streaming conductance (S)
N	number of ions in the flow field
p	pressure (Pa)
P_{in}	input pumping power (W)
P_{out}	output electric power (W)
Q	flow rate ($m^3\ s^{-1}$)
R	universal gas constant (8.314 J $mol^{-1}\ K^{-1}$)
S	electrical conductivity (S)
T	fluid temperature (K)
$\vec{V}$	fluid flow velocity vector
z	valence of ion
Z	figure of merit of energy conversion

Greek letters

Λ	electrolyte electrical conductivity (S m^{-1})
ε	dielectric permittivity,
ε_0	permittivity of vacuum (8.854×10^{-12} C $V^{-1}\ m^{-1}$)
ϕ	externally applied voltage (V)
η	energy conversion efficiency
μ	fluid viscosity (Pa s)
ρ_e	net charge density (C m^{-3})
σ	surface charge density (C m^{-2})
ψ	electrostatic potential due to surface charge (V)

Subscript

i	ith ion
max	maximum value
1	inlet reservoir
2	outlet reservoir

From thermodynamic point of view, the EK cell can be viewed as an energy conversion process. The input power is the pumping power (product of pressure difference applied and flow rate) and the output is the electrical power (product of streaming potential created and electric current). A pioneering study dealing with electrokinetic energy conversion is the work of Osterle [15]. Based on Osterle's work one-dimensional analysis of electrokinetic energy conversion thermodynamic efficiency has been reported in several studies [13–14,16]. The one-dimensional model is based on the infinitely long channel length, equal ion diffusivity and mobility, and Boltzmann ion distribution assumptions. These assumptions may lead to under or over-predicted energy conversion efficiency.

In order to raise the energy conversion efficiency using the electrokinetic effect, a flow field containing many flow passages must be employed to increase the electric current. These multiple channel structures can be obtained through microfabrication technology, chemical synthesis or natural structures [9–10,17]. In general, these microstructures can be viewed as a charged porous media as they are in contact with a polar medium. Because of the structural characteristics, the charged porous media can be considered as composed of an array of identical parallel charged cylindrical capillaries with micro or nanoscale size. The charge inside the porous media can be considered uniformly distributed on the capillary walls with a certain charge density. From this point of view, it is more appropriate to consider the channel in the energy conversion unit as a charged cylindrical capillary instead of a planar slit or rectangular channel, as investigated in the studies of Daiguji et al. [11–12] and van der Heyden et al. [13–14].

In this study a two-dimensional EK cell model is established and solved numerically. A nanoscale finite-length surface-charged cylindrical capillary including the inlet and outlet reservoirs is considered as the physical domain [11–12,18]. The fundamental equations governing the fluid flow, multi-ion transport and electrical potential distribution are solved simultaneously without the assumptions made in the one-dimensional model. The thermodynamic efficiency results obtained from both the one- and two-dimensional models are compared and discussed.

2. Physical and mathematical models

As shown in Fig. 1, we consider a cylindrical capillary having a radius of a and a length of L. Without loss of generality, the capillary wall is considered negatively charged with a surface charge density of σ. The ends of the capillary are connected to inlet and outlet reservoirs which are assumed to be infinitely large compared with the capillary size. We assume that an aqueous salt solution with bulk molar concentration c_0 entirely fills the system and the system is initially in equilibrium. The physical domain considered in this study is the same as that in the studies of Daiguji et al. [11–12] except that the planar slit is replaced by a cylindrical capillary.

For the EK cell operation, fluid flow is driven by an applied pressure difference and creates an electrical potential difference. This can be described using the pressure and voltage differences between the inlet and outlet reservoirs. As shown in Fig. 1, pressure and potential in the inlet and outlet reservoirs are denoted as ϕ_1, p_1, ϕ_2, p_2, respectively. The externally applied pressure difference is $\Delta p = p_2 - p_1 < 0$ and the created streaming potential is $\Delta\phi = \phi_2 - \phi_1 > 0$. Under such applied pressure difference, the fluid flow direction is from the inlet reservoir to outlet reservoir.

2.1. One-dimensional model of EK cell

The one-dimensional EK cell model has been given in several investigations [13–14,16]. A brief summary based on the results reported by Xuan and Li [16] is given below. Based on the Onsager reciprocal theorem, the relations between the flow rate Q, electric current I, pressure difference Δp, and the voltage difference $\Delta\phi$ for the flow with electrokinetic effect through a channel with any cross-sectional shape can be written as,

$$Q = G(-\Delta p) + M(-\Delta\phi) \quad (1)$$

$$I = M(-\Delta p) + S(-\Delta\phi) \quad (2)$$

where G represents the hydrodynamic conductance, M characterizes the electroosmotic flow rate in Eq. (1) and the streaming

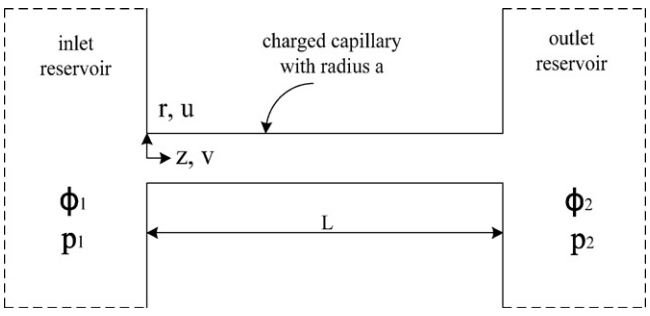

Fig. 1. Schematic of the physical system.

current in Eq. (2), and S represents the electrical conductance. From the energy conversion point of view, the EK cell can be treated as a device that converts the pumping power into electrical power. Referring to Fig. 1, the input pumping power, generated electrical power and energy conversion efficiency can be written as,

$$P_{in} = Q(-\Delta p), \quad P_{out} = I(\Delta\phi), \quad \eta = \frac{P_{out}}{P_{in}} \tag{3}$$

As derived in the study of Xuan and Li [16], the maximum efficiency of EK cell is given as,

$$\eta_{max} = \frac{(1-\sqrt{1-Z})^2}{Z} \tag{4}$$

where Z is called the figure of merit of electrokinetic energy conversion defined as,

$$Z = \frac{M^2}{GS} \tag{5}$$

As indicated in the study of Xuan and Li [16], Z depends on the dimensionless Debye length, zeta potential and a parameter called the Levine number which indicates the nominal ratio of convective to conductive electrical current [19]. It can be said, based on Eqs. (4) and (5), that the maximum EK cell efficiency depends on the electrochemical properties of the working fluid and wall material such as the bulk concentration, electrical conductivity, dielectric constant and zeta potential for flow in a given channel. The maximum efficiency can be obtained for any applied pressure difference since it is independent of the pressure and voltage differences. As noted earlier, Eqs. (1), (2) and (4) are derived under assumptions including an infinitely long channel, equal ionic electrical mobility and Boltzmann ion distribution. These assumptions are removed in the following considering a two-dimensional EK cell model.

2.2. Two-dimensional EK cell model

By assuming that the steady state flow and continuum assumption are valid, the governing equation describing the fluid flow is the modified Navier–Stokes equation written as,

$$\nabla \cdot \vec{V} = 0 \tag{6a}$$

$$\vec{V} \cdot \nabla\vec{V} = -\nabla p + \mu\nabla^2\vec{V} - \rho_e\nabla(\phi+\psi) \tag{6b}$$

where $\vec{V}$ is the fluid flow velocity vector, p is the pressure and μ is the viscosity. The last term on the right-hand side of Eq. (6b) is known as the electric body force per unit volume when electrostriction and the permittivity gradient in the electrical field are ignored. ρ_e is the net charge density defined as,

$$\rho_e = F\sum_{i=1}^{N} z_i c_i \tag{7}$$

where F is the Faraday constant, N is the number of ions in the flow field, c_i and z_i are the molar concentration and the valence of the ith ion, respectively. The potential gradient $\nabla\phi$ results from the potential difference between the inlet and outlet reservoirs, while the potential gradient $\nabla\psi$ results from the electrostatic potential distribution due to the net charge density in the flow field. These two potential fields are described using Laplace and Poisson equations given as,

$$\nabla^2\phi = 0, \quad \nabla^2\psi = -\frac{\rho_e}{\varepsilon\varepsilon_0} \tag{8}$$

where ε is the dielectric permittivity and ε_0 is the permittivity of vacuum. The ion transport in the flow field is governed by the extended Nernst–Planck equation written as,

$$\nabla \cdot [D_i\nabla c_i + m_i z_i c_i \nabla(\phi+\psi) - \vec{V}c_i] = 0 \tag{9}$$

where D_i and m_i are the molecular diffusivity and electrical mobility of the ith ion presented in the system, respectively. For a dilute electrolyte, the ion electrical mobility can be related to the molecular diffusivity by the Nernst–Einstein equation,

$$m_i = \frac{D_i}{RT} \tag{10}$$

where R is the universal gas constant and T is the fluid temperature. Noting that Eqs. (6)–(9) are the general governing equations describing the fluid flow, ion concentration and potential distributions without any assumptions such as Boltzmann distribution and equal ion mobility.

The current flow in the flow field must be computed to evaluate the EK cell efficiency. By knowing the fluid velocity, ion concentration and electrical potential distributions, the current density in the flow field can be calculated as,

$$\vec{i} = -\Lambda\nabla(\phi+\psi) - F\sum z_i D_i \nabla c_i + F\vec{V}\sum z_i c_i \tag{11}$$

where $\Lambda = F^2\sum z_i^2 m_i c_i$ is the electrolyte electrical conductivity. By integrating Eq. (11) through the capillary cross-section, the total current at any cross-section can be obtained. In Eq. (11), the terms on the right-hand side are conductive, diffusive, and the streaming currents, respectively.

All governing equations were written in a cylindrical coordinate system (r,θ,z). Utilizing the symmetry in the θ coordinate, we can recast the problem as an axisymmetric two-dimensional model (r,z). The fluid velocity components in the r- and z-directions are u and v, respectively. The boundary conditions are required to solve Eqs. (6)–(9). Because of the geometrical symmetry, the computational domain is taken as half of the physical domain, as shown in Fig. 2. Since the inlet and outlet reservoirs are relatively large compared with the capillary size, only portions of the reservoirs near the capillary entrance and exit are included in the computation domain. As indicated in Fig. 2, the radius and length of the computation domains in the reservoirs are taken to be A_R and L_R, respectively. As indicated in the studies of Daiguji et al. [11–12] and Mansouri et al. [18], as long as the computational domain size in the reservoirs is large enough, no significant effects in the fluid flow, ion transport and potential distribution will result. Referring to Fig. 2 and taking the outlet reservoir as the pressure and potential references, the boundary conditions for simulating the fluid flow velocity, ion concentration and potential distributions in the EK cell are specified as follows:

Boundary AB:

$$p_1 = -\Delta p, \ \psi = 0, \quad \phi_1 = -\Delta\phi, \ c_i = c_0 \tag{12a}$$

Boundaries BC, FG and AH:

$$\frac{\partial u}{\partial r} = \frac{\partial v}{\partial r} = \frac{\partial\psi}{\partial r} = \frac{\partial\phi}{\partial r} = \frac{\partial c_i}{\partial r} = 0 \tag{12b}$$

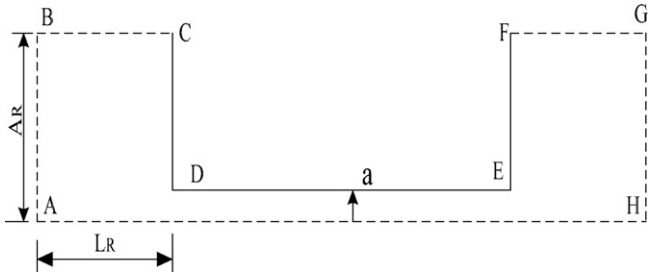

Fig. 2. Computational domain.

Boundaries CD and FE:

$$u = 0, v = 0, \frac{\partial c_i}{\partial z} = \frac{\partial \psi}{\partial z} = \frac{\partial \phi}{\partial z} = 0 \quad (12c)$$

Boundary DE:

$$u = 0, v = 0, \quad \frac{\partial \phi}{\partial r} = 0, \quad \frac{\partial \psi}{\partial r} = -\frac{\sigma}{\varepsilon\varepsilon_0}, \quad \frac{\partial c_i}{\partial r} = 0 \quad (12d)$$

Boundary GH:

$$p_2 = 0, \quad \psi = 0, \quad \phi_2 = 0, \quad c_i = c_0 \quad (12e)$$

As shown in Fig. 2, boundaries AB, BC, FG and GH are used to emulate the infinitely large reservoirs. Because boundaries AB and GH are far away from the capillary inlet and exit, therefore the pressure, potential and ion concentration values are equal to those of bulk fluid inside the reservoirs. At the BC and FG boundaries, the fluid velocity, ion concentration and potential gradients in radial direction are specified to be zero to emulate the infinite large reservoirs. The CD and EF boundaries are the reservoir walls. It is assumed the reservoir walls are electrically insulated and no ion deposition occurs. For the boundary condition at the charged wall, as shown in Eq. (12e), we assume that inside the Stern layer the ions are rigidly held and do not contribute to the ionic distribution. The surface charge density satisfies the electroneutrality condition at the wall.

3. Numerical model

Eqs. (6)–(9) along with the boundary conditions given in Eq. (12) were solved using the commercial code Comsol 3.3 (http://www.comsol.com/). The finite element calculations were performed using quadratic triangular elements. Since the accuracy of the numerical solutions strongly depends on the mesh size, a refined mesh is necessary in the region near the surface where the dependent variable gradients are pronounced. A finer mesh is used near the charged surface to capture the subtle changes in the ion concentration and electrical potential. Solution independence on the mesh size was carefully studied before reporting the final results. The numerical results show that the solutions become mesh-independent when the element number exceeds approximately 6000. Hence, the results presented in this study were all obtained using a mesh containing 14,000–20,000 elements.

4. Results and discussion

KCl aqueous solutions at temperature $T = 298$ K were used as the working fluid. The dielectric constant of the KCl aqueous solution is 80, the molecular diffusivities of K^+ and Cl^- ion are 1.96×10^{-9} and 2.03×10^{-9} m^2 s^{-1}, respectively. The density and viscosity of the solution are assumed to be 1000 kg m^{-3} and 10^{-3} Pa s, respectively. The ranges of bulk concentration c_0, capillary radius a and surface charge density σ are chosen as 10^{-5}–10^{-2} M, 10–100 nm and -0.25×10^{-4} to -5×10^{-3} C m^{-2}, respectively. The length of the capillary is fixed with $L = 5$ μm. The size of computational domain in the reservoirs is fixed as $A_R \times L_R = 1$ μm $\times$ 1 μm. For the chosen capillary radius and bulk concentration ranges, the corresponding dimensionless Debye length $\kappa a (\kappa a = a(\varepsilon\varepsilon_0 RT/(2c_0F^2)^{1/2})$ is ranged from 0.1 to 30.

To verify the correctness of the proposed numerical model, the maximum streaming potential denoted as $\Delta\phi_{max}$ computed from the present numerical model is compared with that reported in the study of Daiguji et al. [11] using the same planar slit with a height of 30 nm. The boundary conditions for the planar slit are the same as those shown in Eq. (12) except that the coordinate system is changed from (r,z) to (x,y). As shown in Fig. 3, the agreement is very good. Based on this comparison, the numerical model developed in this study is correct and can be extended to study the energy conversion with other physical domains. In Fig. 3, $\Delta\phi_{max}$ for the cylindrical capillary with $a = 15$ nm is also computed under the same parameters. It is seen that the variation trend of $\Delta\phi_{max}$ is similar to that of planar slit but with smaller magnitude. This implies that the energy conversion efficiency predicted using the cylindrical capillary would be smaller than that using the planar slit since the efficiency is proportional to $\Delta\phi_{max}$.

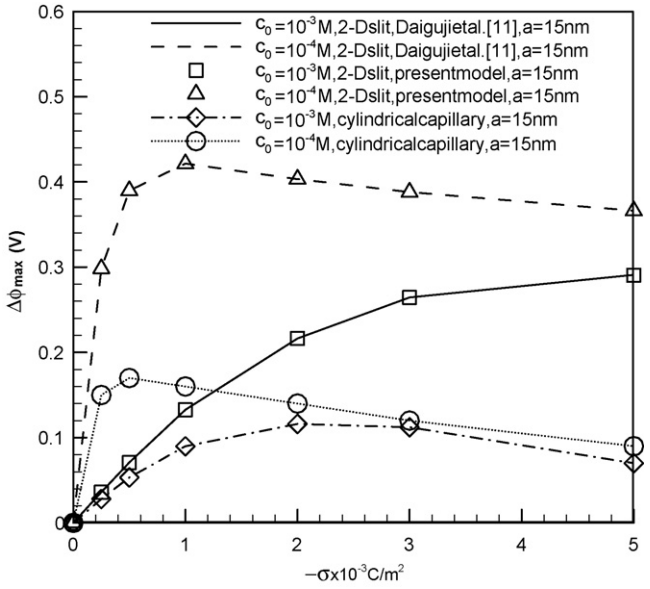

Fig. 3. Comparison of maximum streaming potentials computed from the present numerical model with the results of Daiguji et al. [11] under the same computational domain and numerical parameters.

As discussed in the one-dimensional model, the maximum efficiency of the EK cell is independent from the applied pressure difference, the applied pressure difference is chosen as 500 kPa in this study. The typical results of ion concentration, electric potential, velocity field and current flow in the EK cell are shown in Figs. 4–7 for various streaming potentials. In these results, surface charge density and KCl bulk concentration are fixed as $\sigma = -3 \times 10^{-3}$ C m^{-2} and $c_0 = 10^{-4}$ M, respectively. As shown in Fig. 4, the ion concentration is governed mainly by the surface charge density and the fluid flow. Large variations in ion concentration distribution can be found at the capillary entrance and exit regions. Inside the capillary, concentrations of both K^+ and Cl^- remain constants. The K^+ ion concentration is high in order to balance the negative charges on the wall, while the Cl^- ions are expelled out of the capillary and have a much lower concentration compared with the K^+ ions. Fig. 5 shows the combined electrical potential $(\phi + \psi)$ along the centerline and across the capillary cross-section at $z = 3.5$ μm. As shown in Fig. 5(a), the combined electric potential linearly increases from the inlet to outlet reservoirs and the fluid flow does not affect the potential distribution significantly except at the capillary entrance and exit because of geometric change. For the $\Delta\phi = 0$ case, electric potential can still be found because of the variation in electrostatic potential ψ. Fig. 5(b) shows the combined electric potential profiles across the capillary cross-section at $z = 3.5$ μm. Because the potential in the outlet reservoir is chosen as the reference and the surface charge density is negative, the combined electric potential has a negative value. Note that the potential profile for the $\Delta\phi = 0$ case is due to electrostatic potential only. The axial velocity along the capillary centerline shown in Fig. 6(a) becomes a constant for all the streaming potentials studied indicating the flow becomes fully developed inside the capillary. The

fully-developed velocity profiles taken at $z = 3.5\ \mu m$ are shown in Fig. 6(b). Since the streaming potential results in an electroosmotic flow with direction opposite to the pressure driven flow, the velocity is reduced as the streaming potential increases. This is known as the electroviscous effect. In Fig. 7(a), the current density along the capillary centerline has a constant value inside the capillary showing that the current flow has also become fully developed. The fully developed current density profile at $z = 3.5\ \mu m$ shown in Fig. 7(b) indicates that the current flow has a direction opposite to the fluid flow in the region near the wall. In this region, the K^+ ions are dominated due to the negative surface charge and the fluid velocity is slow due to the no-slip boundary condition at the wall. Because of the electric potential distribution shown in Fig. 5, conductive current with direction opposite to the streaming current is larger than the streaming current and results in negative current flow.

Using the results shown in Figs. 6 and 7, one can construct the electric current–voltage curve (I–V curve) and flow rate–voltage curve (Q–V curve) of the EK cell. Fig. 8 shows the I–V and Q–V curves

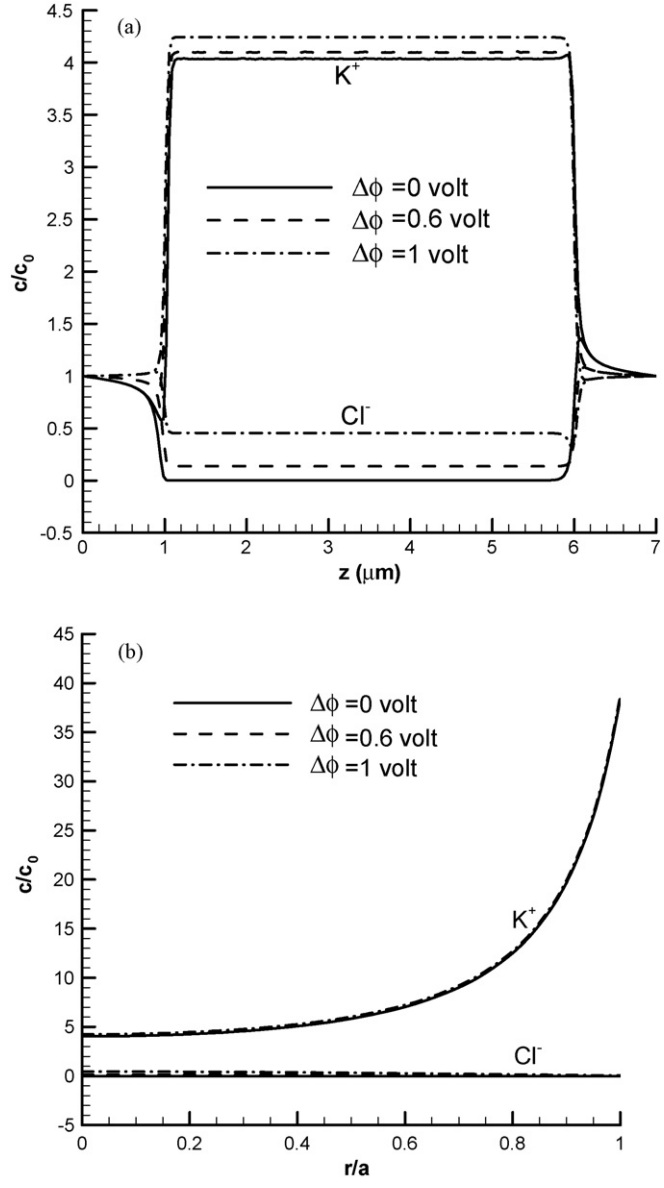

Fig. 4. Ion concentration distributions in EK cell under various streaming potentials. $c_0 = 10^{-4}$ M, $a = 50$ nm, $\sigma = -3 \times 10^{-3}$ C m^{-2}, $\Delta p = -500$ kPa. (a) Along the centerline. (b) Cross-section at $z = 3.5\ \mu m$.

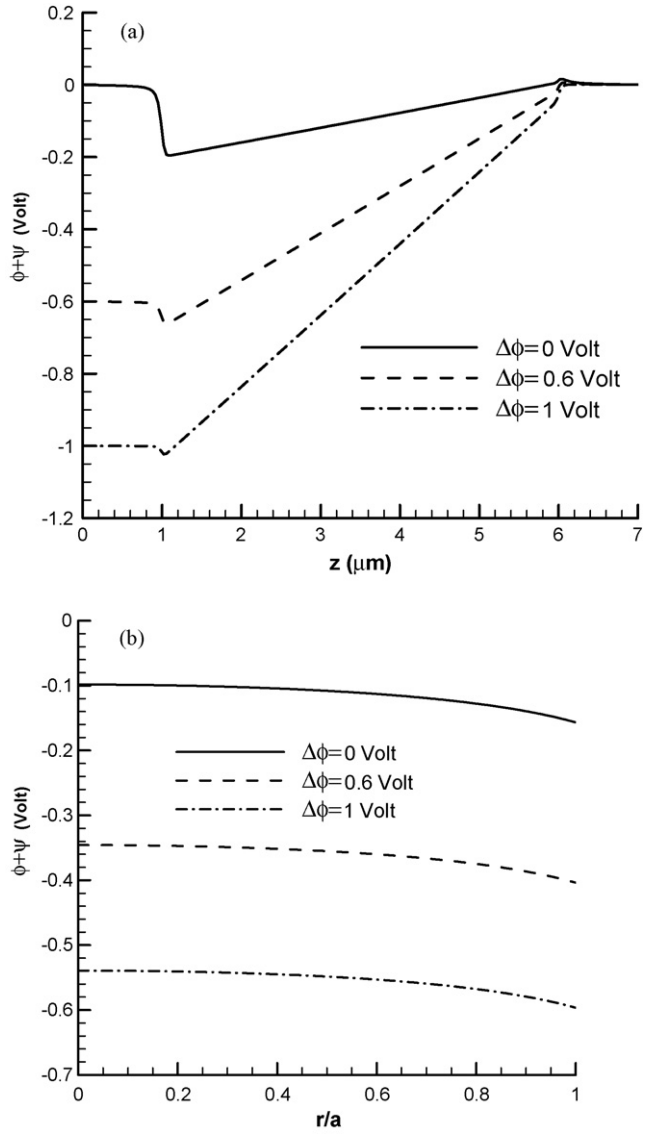

Fig. 5. Combined electric potential ($\phi + \psi$) distributions in EK cell under various streaming potentials. $c_0 = 10^{-4}$ M, $a = 50$ nm, $\sigma = -3 \times 10^{-3}$ C m^{-2}, $\Delta p = -500$ kPa. (a) Along the centerline. (b) Cross-section at $z = 3.5\ \mu m$.

for various bulk concentrations with $a = 50$ nm, $\sigma = -3 \times 10^{-3}$ C m^{-2} and $\Delta p = -500$ kPa. The electrical current and flow rate are obtained by integrating the velocity and current density profiles over the capillary cross-section shown in Figs. 6 and 7(b). From the results shown in Fig. 8, the I–V and Q–V curves are linear when $c_0 = 10^{-3}$ M. As c_0 decreases further to 10^{-5} M, nonlinear I–V and Q–V curves are resulted. As shown in Fig. 8(a), the current magnitude is relatively small compared with other bulk concentrations shown in Fig. 8(a). The reason for this result will be discuss later. Similar to the I–V curves, nonlinear Q–V curve is found when c_0 is low as shown in Fig. 8(b). Fig. 8(b) also shows that the effect of streaming potential and bulk concentration on flow rate is not significant since the flow rate varies in a small range.

From the I–V and Q–V curves, maximum streaming potential $\Delta\phi_{max}$, maximum current I_{max} and maximum flow rate Q_{max} can be found. In Fig. 9, $\Delta\phi_{max}$, I_{max} and Q_{max} as functions of c_0 and σ under the conditions of $\Delta p = -500$ kPa and $a = 50$ nm are presented. Under the zero current condition, $\Delta\phi_{max}$ can be found and shown in Fig. 9(a). It is seen that $\Delta\phi_{max}$ increases with the increase in σ when c_0 are 10^{-2} and 10^{-3} M. When c_0 reduces to 10^{-4} and 10^{-5} M, $\Delta\phi_{max}$

is found to increase to a maximum value and then to decrease with the increase in σ. The variation trend of $\Delta\phi_{max}$ shown in Fig. 9(a) agrees well with that predicted in the study of Daiguji et al. [11]. I_{max} and Q_{max} are obtained under the $\Delta\phi = 0$ condition. Similar to the $\Delta\phi_{max}$, I_{max} is found increase with the increase of σ when c_0 are equal to 10^{-2} and 10^{-3} M as shown in Fig. 9(b). When c_0 are 10^{-4} and 10^{-5} M, I_{max} is found to increase to a maximum value and then to decrease with the increase in σ. The variation in Q_{max} as functions of c_0 and σ are shown in Fig. 9(c). For cases of c_0 equal to 10^{-2} and 10^{-3} M, Q_{max} remains approximately constant as σ increases. For c_0 equal to 10^{-4} and 10^{-5} M, Q_{max} is found to decrease with the increase in σ.

The physical reason for the results shown in Fig. 9 was explained in detail in the studies of Daiguji et al. [11–12] from the variation in ionic distribution characteristics. An alternative explanation is given from the variations in electric potential and streaming current density distributions in this study. As shown in Fig. 10(a), the electrical potential variation along the capillary exists when $\Delta\phi = 0$.

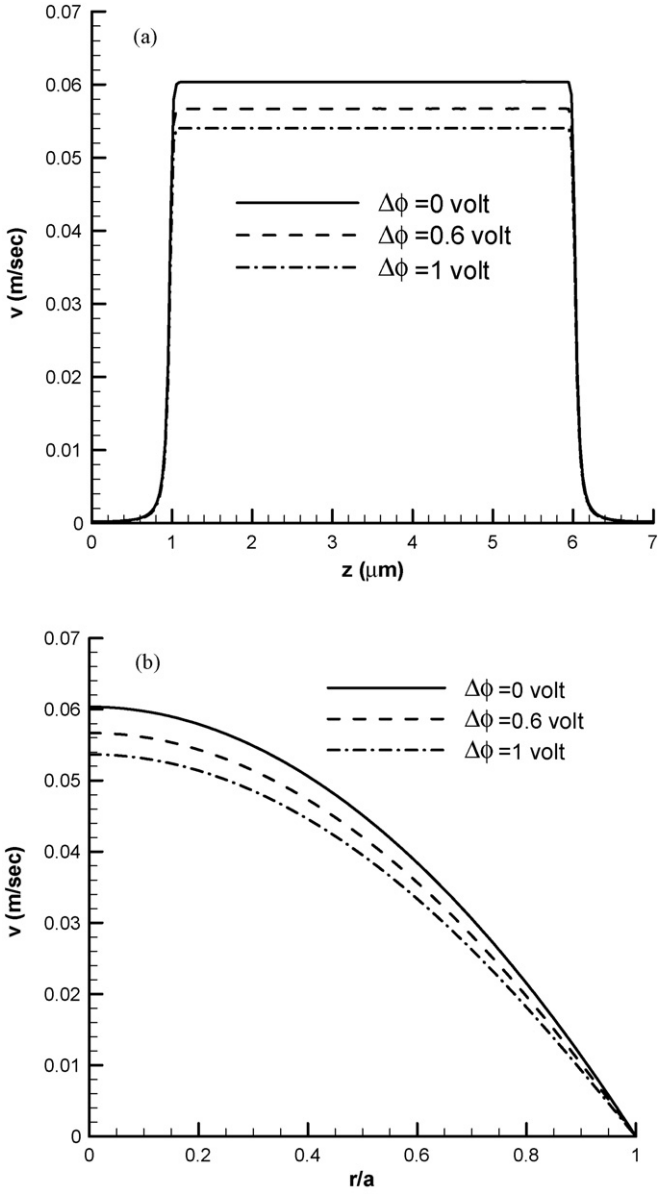

Fig. 6. Fluid flow velocity variations in EK cell under various streaming potentials. $c_0 = 10^{-4}$ M, $a = 50$ nm, $\sigma = -3 \times 10^{-3}$ C m^{-2}, $\Delta p = -500$ kPa. (a) Along the centerline. (b) Cross-section at $z = 3.5$ μm.

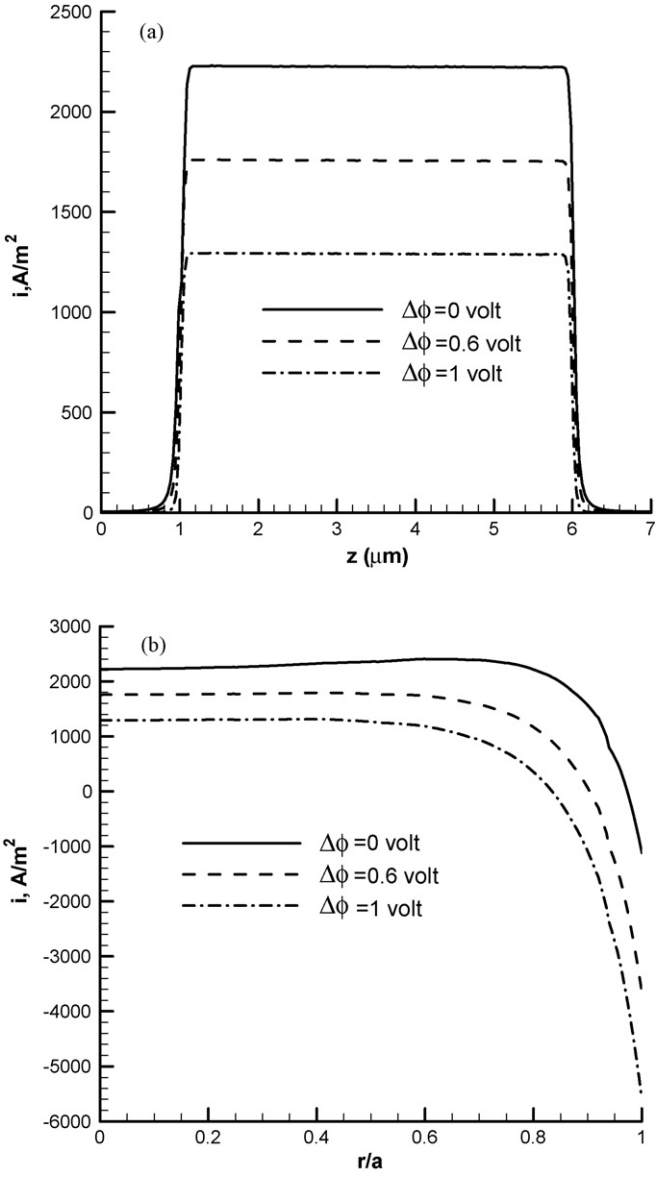

Fig. 7. Electric current variations in EK cell under various streaming potentials. $c_0 = 10^{-4}$ M, $a = 50$ nm, $\sigma = -3 \times 10^{-3}$ C m^{-2}, $\Delta p = -500$ kPa. (a) Along the centerline. (b) Cross-section at $z = 3.5$ μm.

Since $\Delta\phi$ is zero, this potential variation is obviously contributed by the electrostatic potential which is produced by the ion concentration change at the capillary entrance and exit and the fluid flow. Fig. 10(a) also shows that the electrostatic potential magnitudes and its gradient increase with the decrease in c_0. The effect of this electrostatic potential gradient is to produce a conductive electric current opposite to the streaming current. Fig. 10(b) shows the electrical current density profiles across the capillary cross-section under the $\Delta\phi = 0$ condition. Because of the electrostatic potential gradient, conductive current with direction opposite to the streaming current appears. In the near-wall region, negative electric current is found because of strong conductive current and weak streaming current.

Note that the electrostatic potential gradient exists not only when $\Delta\phi = 0$ but also in the non-zero $\Delta\phi$ cases. This implies that the existence of electrostatic potential gradient in the flow field will reduce the current magnitude, especially when the bulk concentration is low. The electrostatic potential gradient appearance explains the significant reductions in current in the I–V curve shown

in Fig. 8(a) and maximum current I_{max} shown in Fig. 9(b) when the bulk concentration is low. From the streaming potential theory, maximum streaming potential is obtained when the total current is zero. Based on the above discussion on the electric current characteristics, nonlinear variation of maximum streaming potential as function of surface charge density for low bulk concentrations is expected, as shown in Fig. 9(a). In the one-dimensional model, the potential gradient due to the electrostatic potential variation does not appear since the capillary is assumed to be infinitely long and without considering the inlet and outlet reservoirs. Overestimated energy conversion is expected from the one-dimensional model.

From the I–V and Q–V curves discussed above, the energy conversion efficiency of the EK cell can be computed using Eq. (3). In Fig. 11, the EK cell efficiencies as a function of the streaming potential under various bulk concentrations are shown. When $\Delta\phi/\Delta\phi_{max} = 0$ and $\Delta\phi/\Delta\phi_{max} = 1$, the efficiencies are zero because of zero stream-

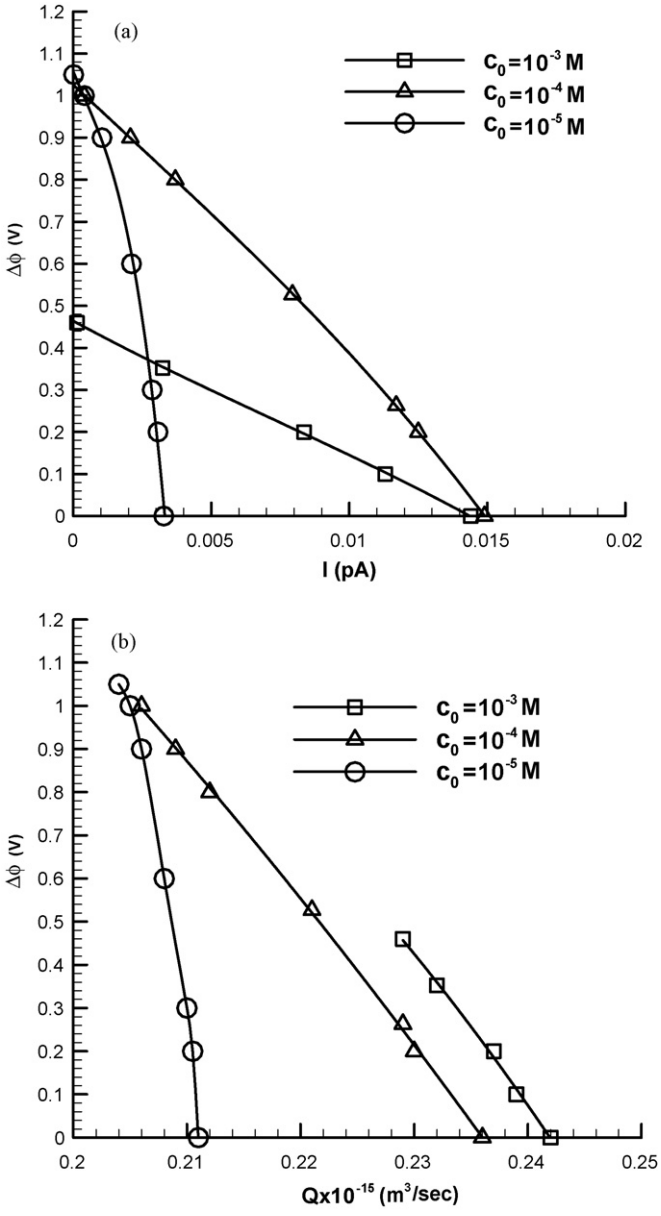

Fig. 8. Electric current–voltage (I–V) curves and flow rate–voltage (Q–V) curves of EK cell for various KCl bulk concentrations. $a = 50$ nm, $\sigma = -3 \times 10^{-3}$ C m^{-2}, $\Delta p = -500$ kPa. (a) I–V curves. (b) Q–V curves.

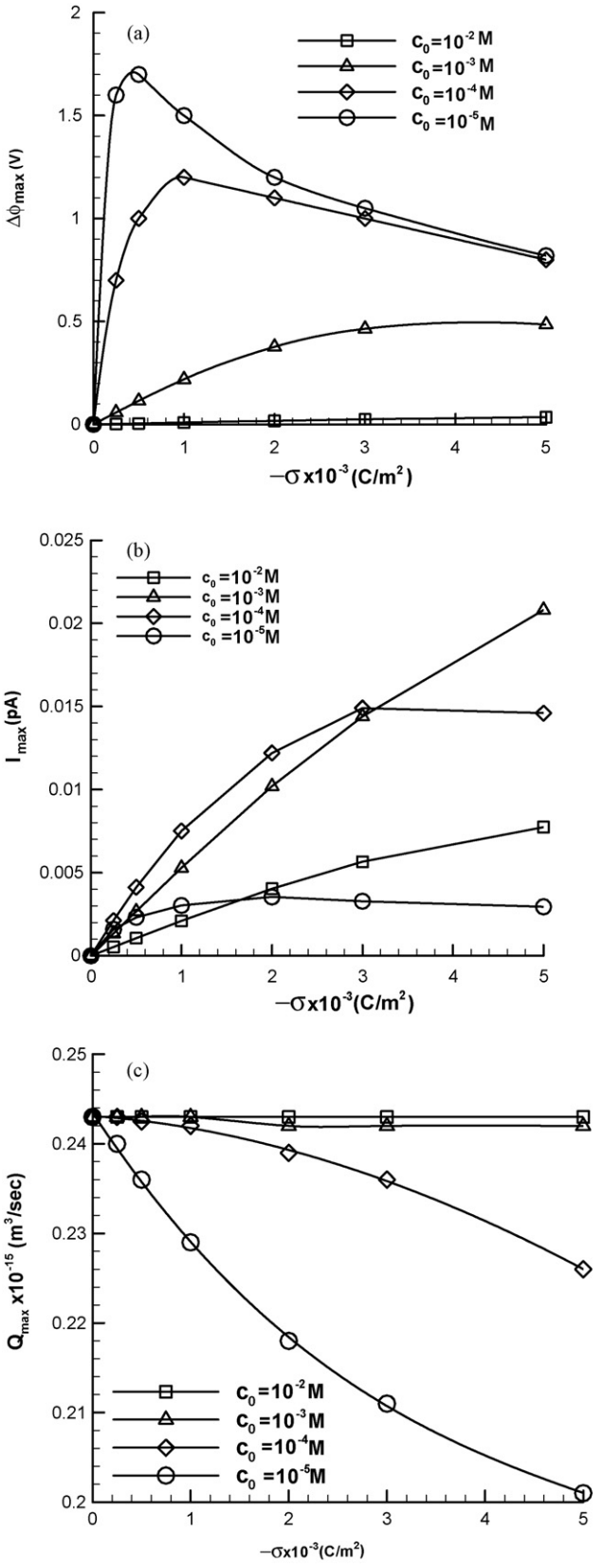

Fig. 9. Maximum streaming potential $\Delta\phi_{max}$, maximum electric current I_{max} and maximum flow rate in EK cell as functions of surface charge density and KCl bulk concentration. $a = 50$ nm, $\Delta p = -500$ kPa. (a) Streaming potential. (b) Electric current. (c) Flow rate.

ing potential and zero current, respectively. The efficiency profiles are all in parabolic shape and maximum efficiency depends on the bulk concentration and streaming potential. For the case of $c_0 = 10^{-3}$ and 10^{-4} M, maximum efficiency occurs at about $\Delta\phi/\Delta\phi_{max} = 0.5$. For $c_0 = 10^{-5}$ M, the maximum efficiency occurs approximately at $\Delta\phi/\Delta\phi_{max} = 0.7$ because of the nonlinear *I–V* curve.

The results shown in Fig. 11 indicate that the maximum energy conversion efficiency occurs when $c_0 = 10^{-4}$ M, $a = 50$ nm, $\sigma = -3 \times 10^{-3}$ C m^{-2}, $\Delta p = -500$ kPa and $\Delta\phi/\Delta\phi_{max} = 0.5$. A more detail of the maximum energy conversion efficiency is given in Fig. 12 in which the maximum energy conversion efficiency as functions of the bulk concentration, surface charge density and capillary radius are presented and compared with the one-dimensional model predictions described in Eq. (4). The dimensionless Debye length κa is also indicated in Fig. 12. In Fig. 12(a), the maximum efficiencies with $c_0 = 10^{-2}$ M are shown for capillary radii $a = 10$, 50 and 100 nm. The maximum efficiency increases with the increasing surface charge density and decreasing capillary radius. The agreement between the one- and two-dimensional models is good for the

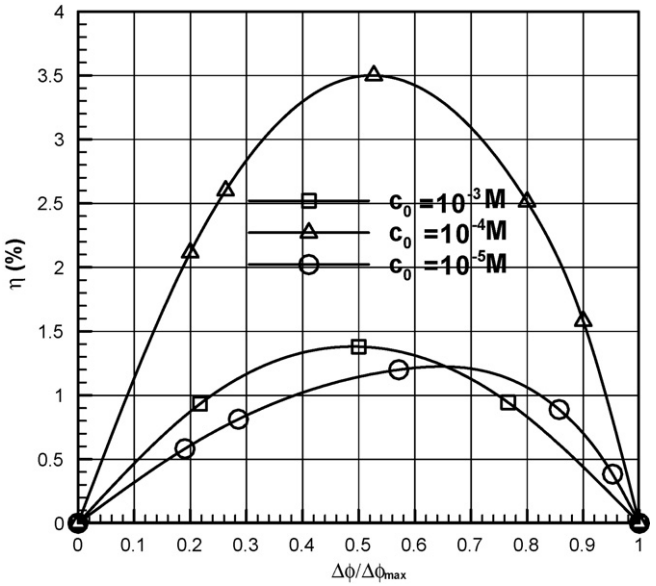

Fig. 11. Thermodynamic efficiency of EK cell as function of KCl bulk concentration and streaming potential. $a = 50$ nm, $\sigma = -3 \times 10^{-3}$ C m^{-2} and $\Delta p = -500$ kPa.

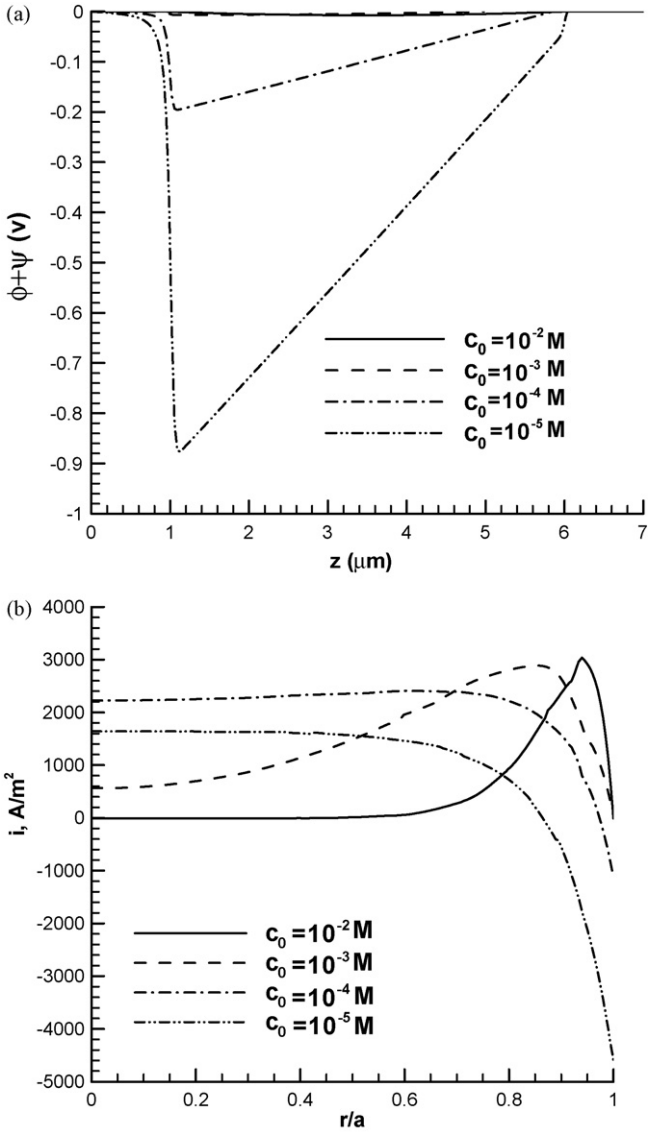

Fig. 10. Combined electric potential distribution along the capillary centerline and current density profiles at $z = 3.5$ μm as function of KCl bulk concentration under the conditions of $\Delta\phi = 0$, $a = 50$ nm, $\sigma = -3 \times 10^{-3}$ C m^{-2} and $\Delta p = -500$ kPa. (a) Potential. (b) Current density.

surface charge density and capillary radius ranges studied. Small discrepancy exists for the case of $a = 10$ nm. For the $c_0 = 10^{-3}$ M case shown in Fig. 12(b), maximum efficiency also increases with the increasing surface charge density and decreasing capillary radius. Good agreement between the one- and two-dimensional predictions can still be obtained for the cases of $a = 50$ and 100 nm ($\kappa a = 5.21$ and 10.04) for the surface charge density range studied. For the case of $a = 10$ nm ($\kappa a = 1.04$), small deviation between the one- and two-dimensional models appears. For the case of $c_0 = 10^{-4}$ M shown in Fig. 12(c), the maximum efficiency increases to a maximum value and then decreases slightly as the surface charge density increases. It is also found that the efficiency for $a = 10$ nm becomes smaller than the $a = 50$ and 100 nm cases. The agreement between one- and two-dimensional models can only be found when κa is large and surface charge density is small. For small κa and large surface charge density cases, deviation between the one- and two-dimensional models becomes significant. When the bulk concentration is further reduced to 10^{-5} M as shown in Fig. 12(d), the variation trends for the maximum efficiency are approximately similar to those found for $c_0 = 10^{-4}$ M case but with smaller magnitudes and more significant drops in the high surface charge density range. The predictions between one- and two-dimensional models completely disagree. Since the assumptions made in the one-dimensional model have been removed in the two-dimensional model, the results obtained from the two-dimensional model are considered to be more realistic in predicting the electrokinetic energy conversion performance. From the results shown in Fig. 12, it is seen that the one-dimensional model is valid only for large κa and small surface charge density.

Since the efficiency is evaluated based on the variations in current, streaming potential and flow rate, we use the results for the $a = 50$ nm case to explain the observations shown in Fig. 12 in more detail. In Fig. 9, typical results of maximum streaming potential, current and flow rate are shown. Since the applied pressure difference is fixed as $\Delta p = -500$ kPa and flow rate remains approximately constant, the maximum efficiency would be proportional to the magnitude of maximum power output $\Delta\phi_{max} I_{max}$. For $c_0 = 10^{-2}$ and 10^{-3} M cases, both $\Delta\phi_{max}$ and I_{max} increase with the surface charge density. Therefore, the maximum efficiency increases with

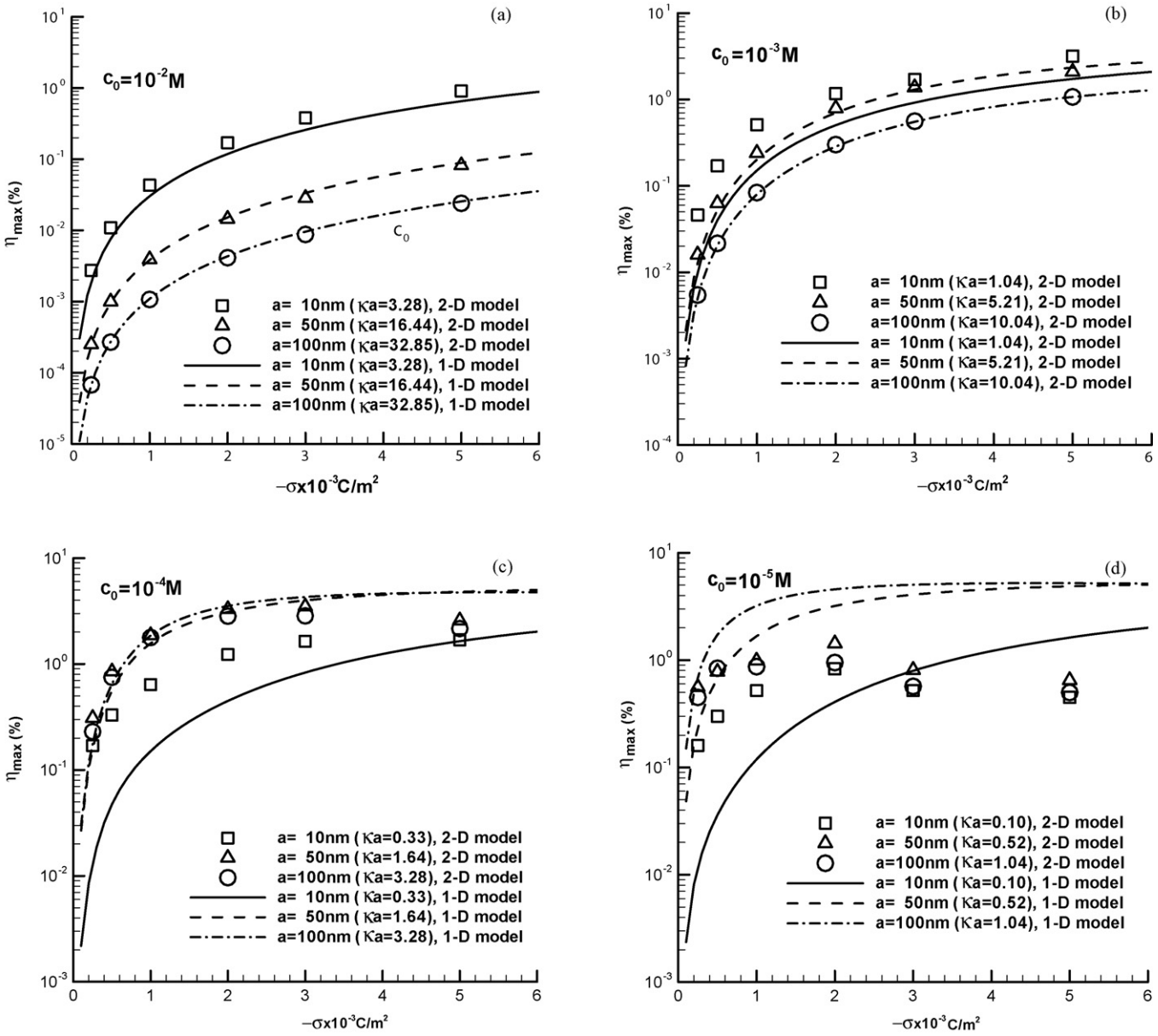

Fig. 12. Maximum efficiencies as functions of KCl bulk concentration, capillary radius and surface charge density. (a) $c_0 = 10^{-2}$ M. (b) $c_0 = 10^{-3}$ M. (c) $c_0 = 10^{-4}$ M. (d) $c_0 = 10^{-4}$ M.

the increase in surface charge density as indicated in Figs. 12(a and b). For $c_0 = 10^{-4}$ and 10^{-5} M cases, variations of $\Delta\phi_{max}$ and I_{max} become nonlinear with respect to the surface charge density. The resulting maximum efficiency also varies nonlinearly with the surface charge density. Because of the decreases in $\Delta\phi_{max}$ and I_{max} when the surface charge density is large, the maximum efficiencies for these two bulk concentrations also decrease when the surface charge is high, as shown in Fig. 12(c and d).

Fig. 13 shows the maximum efficiency as a function of κa for various surface charge densities to provide better understanding of the maximum efficiency dependence on κa. It is seen that an optimum maximum efficiency occurs when κa is equal to 2 and its magnitude increases with the increase in surface charge density.

Besides the EK cell, another important application of electrokinetic effect is the electrokinetic pump (EK pump) [20,21]. Since the EK pump operation is the reverse of the EK cell, the current numerical model can be easily extended to the 2D simulation of EK pump. In EK pump, the fluid flow is driven by an applied voltage and a pressure rise is created in the flow direction. Similar to the EK cell case, EK pump operation can be described by using the pressure and voltage differences between the inlet and outlet reservoirs. Referring to Fig. 1, pressure and potential in the inlet and outlet reservoirs are denoted as ϕ_1, p_1, ϕ_2, p_2, respectively. Using the current established model to simulate the EK pump, an externally applied voltage $\Delta\phi = \phi_2 - \phi_1 < 0$ and a back pressure $\Delta p = p_2 - p_1 > 0$ are specified at the inlet and outlet reservoirs. Referring to Fig. 2, the boundary conditions needed to be changed are

Boundary AB:

$$p_1 = 0, \psi = 0, \phi_1 = -\Delta\phi, c_i = c_0$$

Boundary GH:

$$p_2 = \Delta p, \phi_2 = 0, \psi = 0, c_i = c_0$$

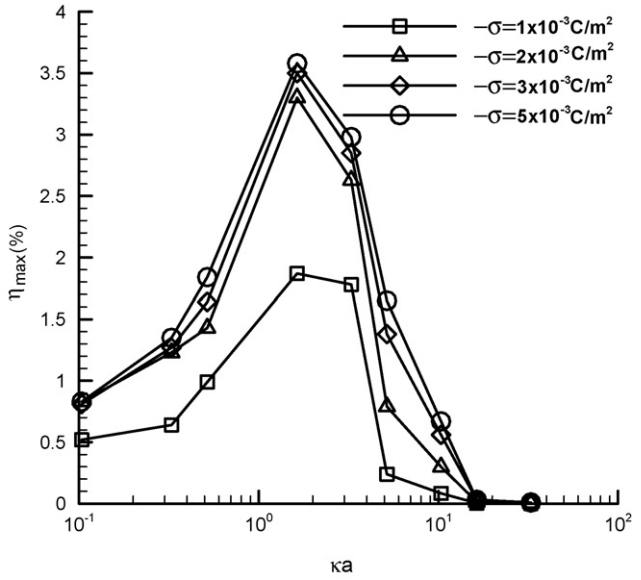

Fig. 13. Maximum efficiency as functions of dimensionless Debye length κa for various surface charge densities.

5. Conclusion

The energy conversion efficiency of electrical power generation using the electrokinetic effect was investigated numerically. A two-dimensional axisymmetric physical domain including a finite-length charged cylindrical capillary and reservoirs connected at the capillary ends was considered. The fluid flow velocity, ion concentration and electrical potential were solved simultaneously based on Navier–Stokes, Nernst–Planck, Laplace and Poisson equations. Using the computed velocity, ion concentration and electrical potential distributions, the electrical current flow in the capillary was computed.

For the bulk concentration, capillary radius and surface charge density in the ranges of 10^{-5}–10^{-2} M, 10–100 nm and -0.25×10^{-4} to -5×10^{-3} C m^{-2}, the two-dimensional computational results show that the electrostatic potential gradient produced by the changes in ion concentration at the capillary entrance and exit and fluid flow plays an important role in evaluating EK cell efficiency. It was found that the electrostatic potential gradient produces a conductive current in direction opposite that to the streaming potential, in addition to that produced by the streaming potential. It was also found that the conductive current produced by the electrostatic potential gradient increased with the decrease in bulk concentration and increase in surface charge density. In terms of the dimensionless Debye length κa, this indicated that the electrostatic potential gradient is large when κa is small. In the one-dimensional model, the electrostatic potential gradient cannot be predicted because the capillary inlet and exit are excluded. This implies that the electrical current predicted from the one-dimensional model would be higher than that predicted from the two-dimensional model.

Because of the conductive current produced by the electrostatic potential gradient, the total current is reduced in the flow field. The computed results show that current–voltage curve (I–V curve) and flow rate–voltage curve (Q–V curve) become nonlinear when the bulk concentration is low. Using the I–V and Q–V curves, the maximum EK cell efficiency is evaluated. For high bulk concentration cases, it was found that maximum efficiency increased with the increase in surface charge density. For low bulk concentration cases, the maximum efficiency increased to a maximum value and then decreased slightly with respect to the increase in surface charge density. The comparison between the maximum efficiencies predicted from one- and two-dimensional models indicated that the one-dimensional model is valid only when κa is large and the surface charge density is low. For small κa and large surface charge cases, the one-dimensional model over-predicted the efficiency because the electrostatic potential gradient is neglected. An optimum maximum efficiency is found when κa is equal to 2 and its magnitude increases with the increase in surface charge density based on the two-dimensional model results.

References

[1] R.B.M. Schasfoort, S. Schlautmann, J. Hendrikse, A. van den Berg, Science 286 (1999) 942.
[2] J.C. Fister, S.C. Jacobson, L.M. Davis, J.M. Ramsey, Anal. Chem. 70 (1998) 431.
[3] B.H. Weigl, P. Yager, Science 283 (1999) 346.
[4] J. Yang, F. Fu, L.W. Kostiuk, D.Y. Kowk, J. Micromech. Microeng. 13 (2003) 963.
[5] J. Yang, F. Fu, L.W. Kostiuk, D.Y. Kowk, Proceedings of the 2004 International Conference on MEMS NANO and Smart Systems, Banff, Alberta, Canada, 2004.
[6] R.F. Probstein, Physicochemical Hydrodynamics: An Introduction, second ed., Wiely, New York, 1994.
[7] R.J. Hunter, Foundations of Colloid Science, Oxford University Press, Oxford, U.K., 2001.
[8] J. Israelachvili, Intermolecular and Surface Forces, second ed., Academic, London, 2003.
[9] W. Olthuis, B. Schippers, J. Eijkel, A. van der Berg, Sens. Actuators B 111–112 (2005) 385.
[10] M.C. Lu, S. Satyanarayana, R. Karnik, A. Majumdar, C.C. Wang, J. Micromech. Microeng. 16 (2006) 667.
[11] H. Daiguji, P. Yang, A.J. Szeri, A. Majumdar, Nano Lett. 4 (12) (2004) 2315.
[12] H. Daiguji, Y. Oka, T. Adachi, K. Shirono, Electrochem. Commun. 8 (2006) 1796.
[13] F.H.J. van der Heyden, D.J. Bonthuis, D. Stein, C. Meyer, C. Dekker, Nano Lett. 6 (100) (2006) 2232.
[14] F.H.J. van der Heyden, D.J. Bonthuis, D. Stein, C. Meyer, C. Dekker, Nano Lett. 7 (4) (2007) 1022.
[15] J.F. Osterle, J. Appl. Mech. 31 (1964) 161.
[16] X. Xuan, D. Li, J. Power Sources 156 (2005) 677.
[17] P. Wang, Z. Chen, H.C. Chang, Sens. Actuators B 113 (2006) 500.
[18] A. Mansouri, C. Scheuerman, S. Bhattacharjee, D.Y. Kwok, L.W. Kostiuk, J. Colloid Interface Sci. 292 (2005) 567.
[19] S.K. Griffiths, R.H. Nilson, Electrophoresis 26 (2005) 351.
[20] S. Yao, A.M. Myers, J.D. Posner, K.A. Rose, J.G. Santiago, J. Microelectromech. Syst. 15 (2006) 717.
[21] Y. Chen, M. Li, Y. Hu, W. Chang, C. Wang, Microfluid Nanofluid (2008) 235.